

NASA/TM—2009-215807



Advanced Noise Control Fan Aerodynamic Performance

Richard F. Bozak, Jr.
Glenn Research Center, Cleveland, Ohio

November 2009

NASA STI Program . . . in Profile

Since its founding, NASA has been dedicated to the advancement of aeronautics and space science. The NASA Scientific and Technical Information (STI) program plays a key part in helping NASA maintain this important role.

The NASA STI Program operates under the auspices of the Agency Chief Information Officer. It collects, organizes, provides for archiving, and disseminates NASA's STI. The NASA STI program provides access to the NASA Aeronautics and Space Database and its public interface, the NASA Technical Reports Server, thus providing one of the largest collections of aeronautical and space science STI in the world. Results are published in both non-NASA channels and by NASA in the NASA STI Report Series, which includes the following report types:

- **TECHNICAL PUBLICATION.** Reports of completed research or a major significant phase of research that present the results of NASA programs and include extensive data or theoretical analysis. Includes compilations of significant scientific and technical data and information deemed to be of continuing reference value. NASA counterpart of peer-reviewed formal professional papers but has less stringent limitations on manuscript length and extent of graphic presentations.
- **TECHNICAL MEMORANDUM.** Scientific and technical findings that are preliminary or of specialized interest, e.g., quick release reports, working papers, and bibliographies that contain minimal annotation. Does not contain extensive analysis.
- **CONTRACTOR REPORT.** Scientific and technical findings by NASA-sponsored contractors and grantees.

- **CONFERENCE PUBLICATION.** Collected papers from scientific and technical conferences, symposia, seminars, or other meetings sponsored or cosponsored by NASA.
- **SPECIAL PUBLICATION.** Scientific, technical, or historical information from NASA programs, projects, and missions, often concerned with subjects having substantial public interest.
- **TECHNICAL TRANSLATION.** English-language translations of foreign scientific and technical material pertinent to NASA's mission.

Specialized services also include creating custom thesauri, building customized databases, organizing and publishing research results.

For more information about the NASA STI program, see the following:

- Access the NASA STI program home page at <http://www.sti.nasa.gov>
- E-mail your question via the Internet to help@sti.nasa.gov
- Fax your question to the NASA STI Help Desk at 443-757-5803
- Telephone the NASA STI Help Desk at 443-757-5802
- Write to:
NASA Center for AeroSpace Information (CASI)
7115 Standard Drive
Hanover, MD 21076-1320

NASA/TM—2009-215807



Advanced Noise Control Fan Aerodynamic Performance

Richard F. Bozak, Jr.
Glenn Research Center, Cleveland, Ohio

National Aeronautics and
Space Administration

Glenn Research Center
Cleveland, Ohio 44135

November 2009

Acknowledgments

The author would like to acknowledge the efforts of the Advanced Noise Control Fan (ANCF) support crew in the Aero-Acoustic Propulsion Laboratory, and also the assistance of Dr. Daniel Sutliff and Dr. Christopher Miller.

Trade names and trademarks are used in this report for identification only. Their usage does not constitute an official endorsement, either expressed or implied, by the National Aeronautics and Space Administration.

This work was sponsored by the Fundamental Aeronautics Program at the NASA Glenn Research Center.

Level of Review: This material has been technically reviewed by technical management.

Available from

NASA Center for Aerospace Information
7115 Standard Drive
Hanover, MD 21076-1320

National Technical Information Service
5285 Port Royal Road
Springfield, VA 22161

Available electronically at <http://gltrs.grc.nasa.gov>

Advanced Noise Control Fan Aerodynamic Performance

Richard F. Bozak, Jr.
National Aeronautics and Space Administration
Glenn Research Center
Cleveland, Ohio 44135

Abstract

The Advanced Noise Control Fan at the NASA Glenn Research Center is used to experimentally analyze fan generated acoustics. In order to determine how a proposed noise reduction concept affects fan performance, flow measurements can be used to compute mass flow. Since tedious flow mapping is required to obtain an accurate mass flow, an equation was developed to correlate the mass flow to inlet lip wall static pressure measurements. Once this correlation is obtained, the mass flow for future configurations can be obtained from the non-intrusive wall static pressures. Once the mass flow is known, the thrust and fan performance can be evaluated. This correlation enables fan acoustics and performance to be obtained simultaneously without disturbing the flow.

List of Symbols

P_s^a	static absolute pressure
P_s^g	static gauge pressure
P_t^a	total absolute pressure
P_t^g	total gauge pressure
P_{atm}	atmospheric pressure
M	mach number
\dot{m}	mass flow
\dot{m}_{corr}	corrected mass flow
T_{amb}	ambient temperature
T_{SD}	standard day temperature
A	duct cross-sectional area
R	gas constant
C	calibration constant
ΔP_{loss}	ICD pressure loss
f	friction factor
ρ	density of air
L	thickness of ICD honeycomb
V	velocity through the ICD
D	effective (pipe) diameter of the ICD area

ν	kinematic viscosity
m	ICD pressure loss equation slope
b	ICD pressure loss equation offset
P_{thrust}	thrust power
P_{shaft}	shaft power
V_{avg}	average duct axial velocity
η	fan efficiency
τ	shaft torque
ω	fan speed

Introduction

The Advanced Noise Control Fan (ANCF) is a 4-ft diameter ducted fan used to measure and evaluate fan noise. It is located in the Aero-Acoustic Propulsion Laboratory (AAPL) at the NASA Glenn Research Center. The ANCF has a nominal inlet duct Mach number of approximately 0.15 when the fan is rotating at 1800 RPM_C. The ANCF has a highly configurable duct arrangement that can be used to evaluate a variety of acoustic technologies (Refs. 1 and 2).

The data presented in this paper were taken from baseline measurements obtained in early 2009, after new rotor blades and a new Inlet Control Device (ICD) were installed (Ref. 3). The ANCF baseline configuration consists of 16 rotor blades at a 28° pitch angle, with 14 stator vanes spaced 1 stator chord length behind the rotor. Along with this baseline configuration, measurements were also taken with the same rotor configuration without stator vanes.

The ANCF offers a variety of static and total pressure probes, which when used with the Electronically Scanned Pressure system (ESP), can obtain very accurate pressure measurements. The ESCORT data acquisition system is used to record the pressure. Along with the pressure measurements, ambient temperature and atmospheric pressure measurements give additional data that is necessary for flow computations. Constant Temperature Anemometry (CTA) measurements measure axial as well as tangential flow. The Probe Actuator and Control System (PACS) is used to position the probes into the flow at different radii.

The versatility of the ANCF duct allows for flow measurements to be taken in different axial locations. In order to correlate inlet duct wall static pressure to mass flow, pressure measurements are taken throughout the ANCF duct. The duct measurement schematic, shown in Figure 2, locates total and static pressure traverses in the inlet and aft sections, as well as a hotfilm traverse to find the swirl angle.

This paper will present the instrumentation, configurations, and equations used to make the mass flow correlation. An accompanying uncertainty analysis will show the quality of the correlation. Beyond the mass flow correlation, the aerodynamic performance of the ANCF rig will be evaluated.

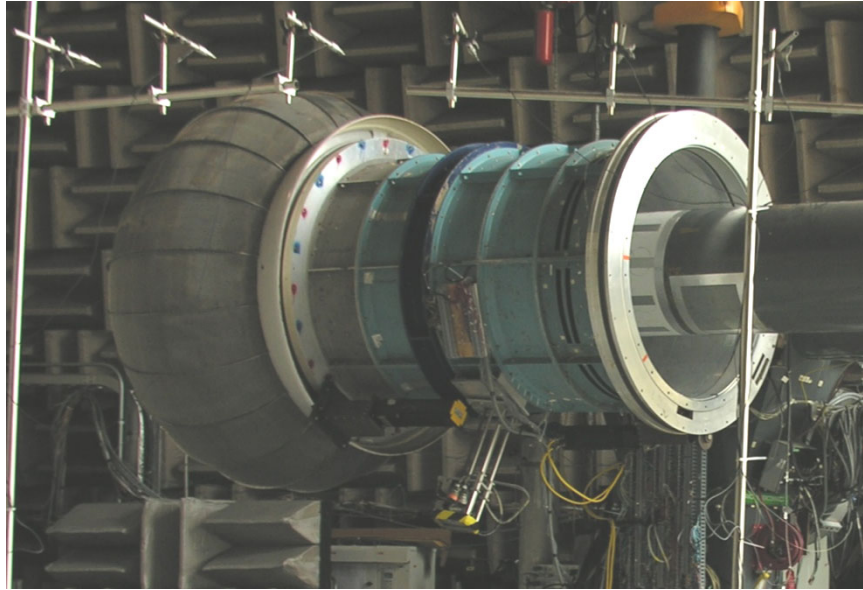


Figure 1.—ANCF Duct

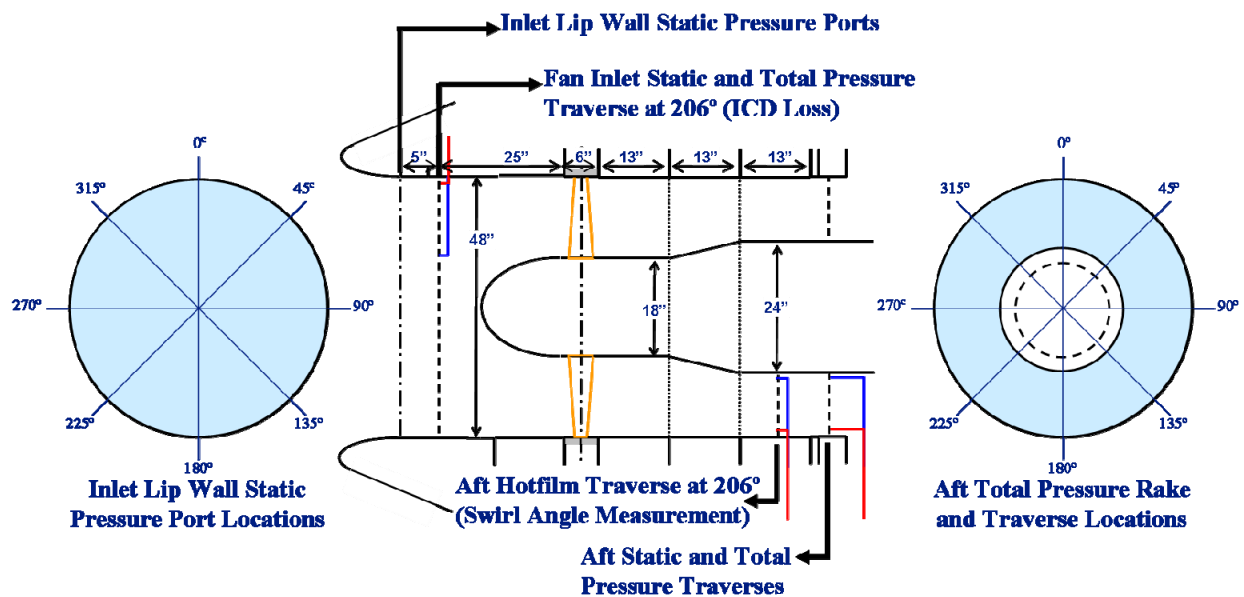


Figure 2.—ANCF Duct Flow Measurement Schematic

Instrumentation

Inlet Lip Wall Static Pressures

The ANCF has eight static pressure ports in the inlet lip. The ports are equally spaced circumferentially around the lip. The inlet lip static pressure ports were designed and installed such that the orifice induced error is negligible (Ref. 4). The cylindrical taps have a 0.0421 in. (1 mm) inner diameter square edge tube insert which is perpendicular to the flow and flush to the duct wall.

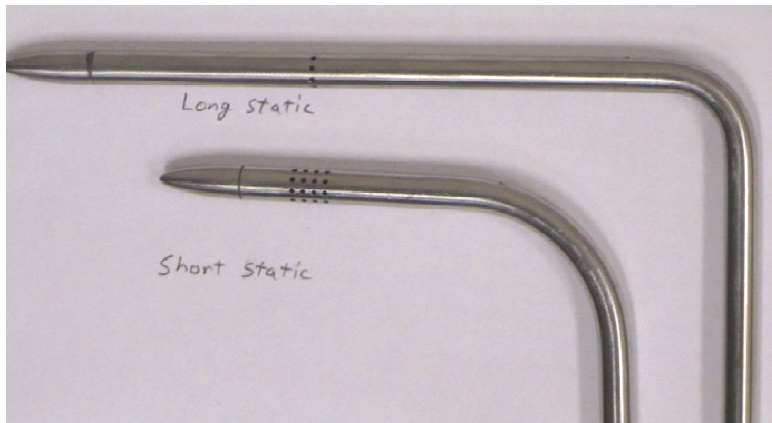


Figure 3.—Short and Long Static Pressure Probes

Static Pressure Probes

Inlet static pressure measurements were taken with a 90° style static pressure probe. The probe has a bullet nose at the leading edge and holes circumferentially located around the tube at the measurement point. This probe measures the static pressure 2-1/4 in. in front of the insertion point. This probe is the “short static” shown in Figure 3.

Aft static pressure measurements were taken with a longer static pressure probe to measure the static pressure 3-1/8 in. in front of the insertion point. Since static pressure probes are sensitive to the yaw angle, the probe was directed into the flow. This probe is the “long static” shown in Figure 3.

Total Pressure Probes

Inlet total pressure measurements were taken with a Kiel type probe (United Sensor KAC-12). This probe has a yaw capture angle of $\pm 52^\circ$.

The aft total pressure measurements used to define the hub and outer wall boundary layers were taken with a total pressure probe with the geometry shown in Figure 4. This probe was rotated into the incoming flow angle to ensure accurate measurements.

Total Pressure Rake

Free-stream aft total pressure measurements were taken with a total pressure rake which consists of six fixed radially spaced Pitot probes. For measurements without stator vanes, the capture angle of these Pitot probes is insufficient due to the $> 25^\circ$ swirl angle. Therefore, an attachment was made to increase the capture angle on the total pressure rake. The geometry of the rake Pitot probes and attachment are shown below in Figure 4. A single Pitot probe with the same geometry as the total pressure rake was tested with and without the attachment in a small flow jet. The results of this test are shown in Figure 5. The yaw capture angle was calculated as being the angle where there is a 1% error in the pressure measurement (Ref. 5). The addition of the probe attachment increased the positive capture angle from approximately 15° up to 21° .

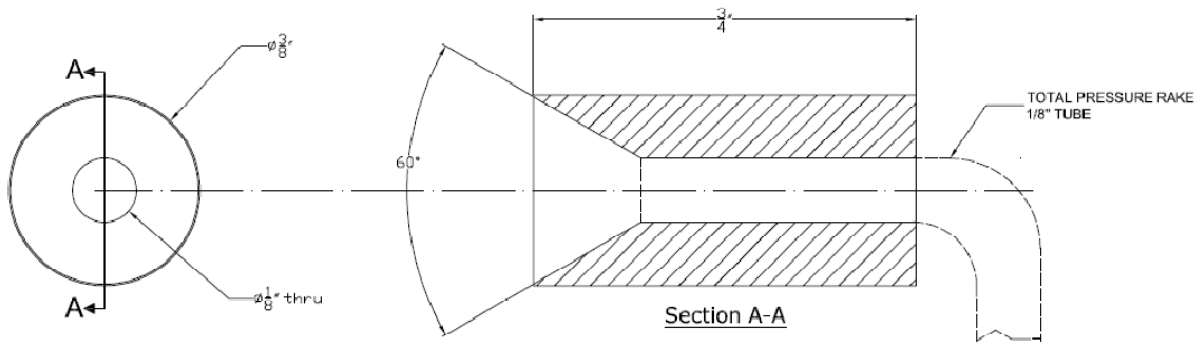


Figure 4.—Drawing of Total Pressure Rake Attachment

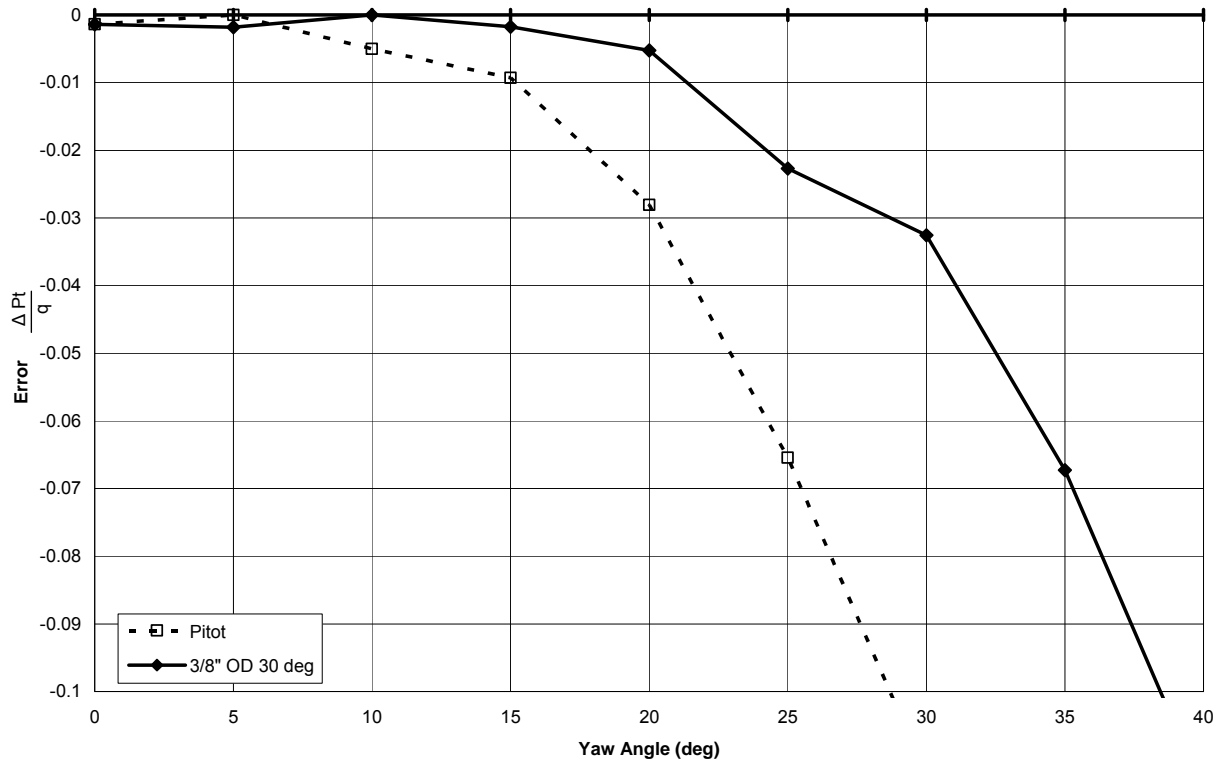


Figure 5.—Total Pressure Probe Yaw Angle Sensitivity

Constant Temperature Anemometry (CTA) Probe

Flow angle measurements were taken with a two-channel hot-film probe. This probe was calibrated with a low-turbulence free jet calibrator. The accuracy of this flow angle measurement primarily depends on the ability to align the probe axially in the ANCF duct.

Motor Measurements

The variable speed motor drive controller outputs the torque delivered by the motor. The fan speed is measured by an encoder on the drive shaft, which is read by a Newport signal conditioner and then by ESCORT.

Equations

The mass flow correlation is based on the relationship of inlet wall static pressure to the mass flow. A ratio was defined to relate the inlet and aft mass flow calculations. This ratio is referred to as the calibration constant. The non-intrusive inlet measurements were used to find an estimated mass flow, while the aft flow mapping gave a measured mass flow. Once the inlet and aft mass flows are calculated, the calibration constant can be found.

$$C = \frac{\dot{m}_{\text{Inlet}}(\text{Estimated})}{\dot{m}_{\text{Aft}}(\text{Measured})} \quad (1)$$

Mass Flow Calculation

The correlation between the inlet wall static pressure and mass flow is based on isentropic and ideal gas assumptions. This correlation is made by comparing the mass flow calculated from the inlet wall static pressure ports and the mass flow calculated from aft pressure measurement maps. At any location in the flow, the local Mach number can be found from the pressure ratio with the following equation.

$$\frac{P_s^a}{P_t^a} = \left(1 + \frac{M^2}{5}\right)^{-\frac{7}{2}} \quad (2)$$

The pressures measured by the inlet wall static pressure ports are proportional to the free stream static pressure. Therefore, this static pressure and free stream total pressure can be used to calculate a Mach number that is proportional to the average inlet duct Mach number. Unlike in the inlet, aft pressure measurements were taken at a variety of radial and circumferential locations to give the Mach number distribution across the exit plane. Once the Mach number is known, the mass flow can be calculated. Using the ideal gas law and speed of sound for an ideal gas with a ratio of specific heats of 1.4 for air, Equation (3) is formulated. All velocities and mass flows presented are corrected to standard day.

$$\dot{m} = P_s^a A \sqrt{\frac{7}{RT_{\text{amb}} \left[\left(\frac{P_s^a}{P_t^a} \right)^{\frac{2}{7}} - 1 \right]}} \quad (3)$$

$$\dot{m}_{\text{corr}} = \sqrt{\frac{T_{SD}}{T_{\text{amb}}}} \dot{m} \quad (4)$$

An estimated inlet mass flow is calculated from the inlet static pressure at the wall, the ICD pressure loss, ambient temperature, and atmospheric pressure measurements. This estimated mass flow is proportional to the measured mass flow. The measured mass flow is calculated from aft pressure measurement maps. The mass flow can be found by dividing the estimated inlet mass flow by the

calibration constant. Flow measurements were taken with corrected fan speeds between 1400 and 2000 rpm to give a range of duct Mach numbers for the mass flow correlation.

ICD Pressure Loss Equation

The ICD adds a pressure drop to the flow path of the ANCF duct. When calculating the mass flow through the inlet, the ICD pressure drop is needed to find the total pressure inside the ICD. Since the mass flow must be calculated using only the inlet lip wall static pressure measurements, an equation was developed to account for the ICD pressure drop. Using the energy equation, a friction loss equation as a function of mass flow was developed for laminar flow through the ICD:

$$\Delta P_{\text{loss}} = f \frac{\rho L V_{\text{avg}}^2}{2D} \quad (5)$$

$$\Delta P_{\text{loss}} = \frac{128\nu L}{\pi D^4} \dot{m} \quad (6)$$

where ΔP_{loss} is the pressure drop across the ICD, ν is the kinematic viscosity of air, L is the thickness of the ICD honeycombs, D is the effective pipe diameter of the entire ICD area, and \dot{m} is the mass flow through the ICD.

Since the geometry of the ICD is constant, the total pressure drop across the ICD is proportional to the mass flow. The small ANCF operating range allows for the relationship between ICD pressure drop and inlet lip wall static pressure to be linearized. A linear equation was fit to the data to obtain an equation for the ICD pressure drop from the inlet wall static pressure.

$$\Delta P_{\text{loss}} = m \cdot P_s^g + b \quad (7)$$

Fan Efficiency Calculation

Once the mass flow is calculated, the performance of the fan can be analyzed. The ANCF is driven by a 200 hp electric motor. The fan's thrust power is a product of the thrust and velocity out of the duct. Instead of calculating a correlation for the velocity, the average velocity is found from correlated mass flow, density, and area. Although the corrected mass flow and velocity are used in the mass flow correlation, the mass flow and velocity are calculated to analyze the fan performance. The fan's output power is calculated from combining thrust and power equations.

$$P_{\text{thrust}} = \frac{1}{2} \dot{m} V_{\text{avg}}^2 \quad (8)$$

The mass flow correlation allows for the fan's output power to be calculated from the inlet duct wall static pressure. Since the fan's efficiency is dependent upon the input power to the fan as well as this output power calculation, the input shaft power is calculated from the fan speed and the torque. The fan speed is measured from an encoder on the fan shaft, while the torque is an output from motor drive controller. The fan efficiency equation, shown below, was used to analyze the performance of the ANCF in a variety of configurations.

$$\text{Thrust} = \dot{m} V_{\text{avg}} \quad (9)$$

$$\eta = \frac{\dot{m} V_{\text{avg}}^2}{2\tau\omega} \quad (10)$$

Mass Flow and Fan Efficiency Equations for ESCORT

In order to calculate mass flow and fan efficiency without detailed flow mapping, equations were developed to be implemented in the ESCORT data acquisition system. The corrected mass flow is calculated from atmospheric and gauge pressure measurements as well as an ambient temperature measurement. The eight circumferentially spaced inlet lip wall static pressure ports were used to divide the inlet flow into eight equally sized areas. The mass flow correlation equation incorporates each of these measurements to obtain the total mass flow.

$$\dot{m}_{\text{corr}} = \sum_{i=1}^8 \left[\frac{(P_{s_i}^g + P_{\text{atm}})A}{8CT_{\text{amb}}} \sqrt{\frac{7T_{SD}}{R} \left[\left(\frac{P_{s_i}^g + P_{\text{atm}}}{mP_{s_i}^g + b + P_{\text{atm}}} \right)^{-\frac{2}{7}} - 1 \right]} \right] \quad (11)$$

Once the corrected mass flow is known, the thrust and fan efficiency can be calculated. The average velocity can easily be found from the corrected mass flow and used to find the thrust. The fan efficiency can then be found by combining Equations (9), (10), and (12) to yield Equation (13).

$$\text{Thrust} = \frac{\dot{m}_{\text{corr}}^2 T_{\text{amb}}^2 R}{AT_{SD} (P_s^g + P_{\text{atm}})} \quad (12)$$

$$\eta = \frac{T_{\text{amb}}^{7/2} \dot{m}_{\text{corr}}^3 R^2}{2A^2 (P_s^g + P_{\text{atm}})^2 T_{SD}^{3/2} \tau\omega} \quad (13)$$

Uncertainty Analysis

Measurement Errors

The measurement uncertainties of each instrument and data acquisition system were examined to determine the total uncertainty of the mass flow correlation. The static and total pressure probes and ports were designed and installed such that the probe error associated with the measurements is negligible (Refs. 4 and 6).

The accuracy of the ESP pressure measurements is $\pm 0.1\%$ of 10 in. of water, which gives an accuracy of ± 0.00036 psi. Along with these gauge pressure measurements, the atmospheric pressure is also measured with an accuracy of ± 0.01 psia and the ambient temperature is measured with an accuracy of ± 0.36 °F. The ESCORT data acquisition system adds an uncertainty of $\pm 0.05\%$ of full scale to the atmospheric pressure and ambient temperature measurements. The total uncertainty on the atmospheric pressure and ambient temperature measurements becomes ± 0.014 psi and ± 0.37 °F respectively.

Aft swirl angles were measured using a 2-channel hotfilm probe. The hotfilm calibration and accompanying data acquisition system errors were judged to be minor compared to the probe installation alignment error. Therefore, the swirl angle accuracy is the probe installation error, which was estimated as $\pm 2^\circ$.

The fan's input power is calculated from torque and fan speed measurements. The motor drive controller outputs the torque, with an accuracy of ± 2.9 ft·lb. The fan speed is measured by an encoder on the drive shaft, which is read by a signal conditioner and ESCORT. The combined accuracy of this measurement is ± 3 rpm.

Calculation Errors

The quality of the mass flow correlation and fan efficiency calculation were analyzed by performing an uncertainty analysis as specified in ASME PTC 19.1 (Ref. 7). Figure 6, below, shows the contributions of the individual measurement errors to the calculation errors. This analysis was done for a nominal corrected fan speed of 1800 rpm. The individual inlet pressure and temperature measurement errors contribute to an uncertainty of ± 0.34 lb_m/s on the inlet lip mass flow calculation. The individual aft measurement uncertainties give an accuracy of ± 2.5 ft/s on the aft corrected velocities as well as an accuracy of ± 2.1 lb_m/s on the calculated aft mass flow. The combination of the calculated inlet and aft mass flows gives an accuracy of ± 0.023 on the calculated calibration constants. Since the calibration constant is the average of four measurements over a range of flows, the entire mass flow correlation has an accuracy of ± 1.6 lb_m/s. When calculating output power of the fan, the velocity and mass flow uncertainties give the power calculation an accuracy of ± 2.2 hp. Since the input power is calculated from the encoder and torque output, it has a combined accuracy of ± 1.0 hp. The combination of input and output power errors gives a combined uncertainty on the efficiency calculation of $\pm 1.9\%$.

Results

Inlet Duct Flow

The inlet pressure traverses were obtained with the short static and Kiel type pressure probes. Figure 8 shows the variation in total and static pressure over the length of the traverse. Since the wall static pressure is significantly lower than the static pressure throughout the traverse, the calibration constant will be greater than 1. The total pressure traverse shows that total pressure measurements 14 in. from the outer wall are sufficiently in the free-stream for ICD pressure drop measurements.

ICD Pressure Drop

The total pressure drop due to the ICD losses was found by measuring the free stream total pressure upstream of the fan with a Kiel type total pressure probe. The relationship between wall static and free stream total pressure for each fan speed and vane configuration at a location of 14 in. from the outer wall is shown below in Figure 8. The linear regression of the data gives a slope of 0.015 and an offset of 0.0007 psig. The error bars show that the linear approximation holds within the uncertainty of the pressure measurements.

Inlet Duct Mass Flow Calculation

The mass flow through the inlet duct was calculated using Equations (3) and (4). The eight static pressure measurements and the free stream total pressure were used to find eight corrected velocities. The duct area was divided into eight equally sized pie shaped areas. The velocities and their corresponding areas were used in conjunction with the density of the air at the measured ambient temperature to obtain the mass flow through each section. Subsequently, the mass flow through the entire inlet is found. The inlet mass flow, corrected to standard day, over a range of corrected fan speeds is shown below in Figure 9.

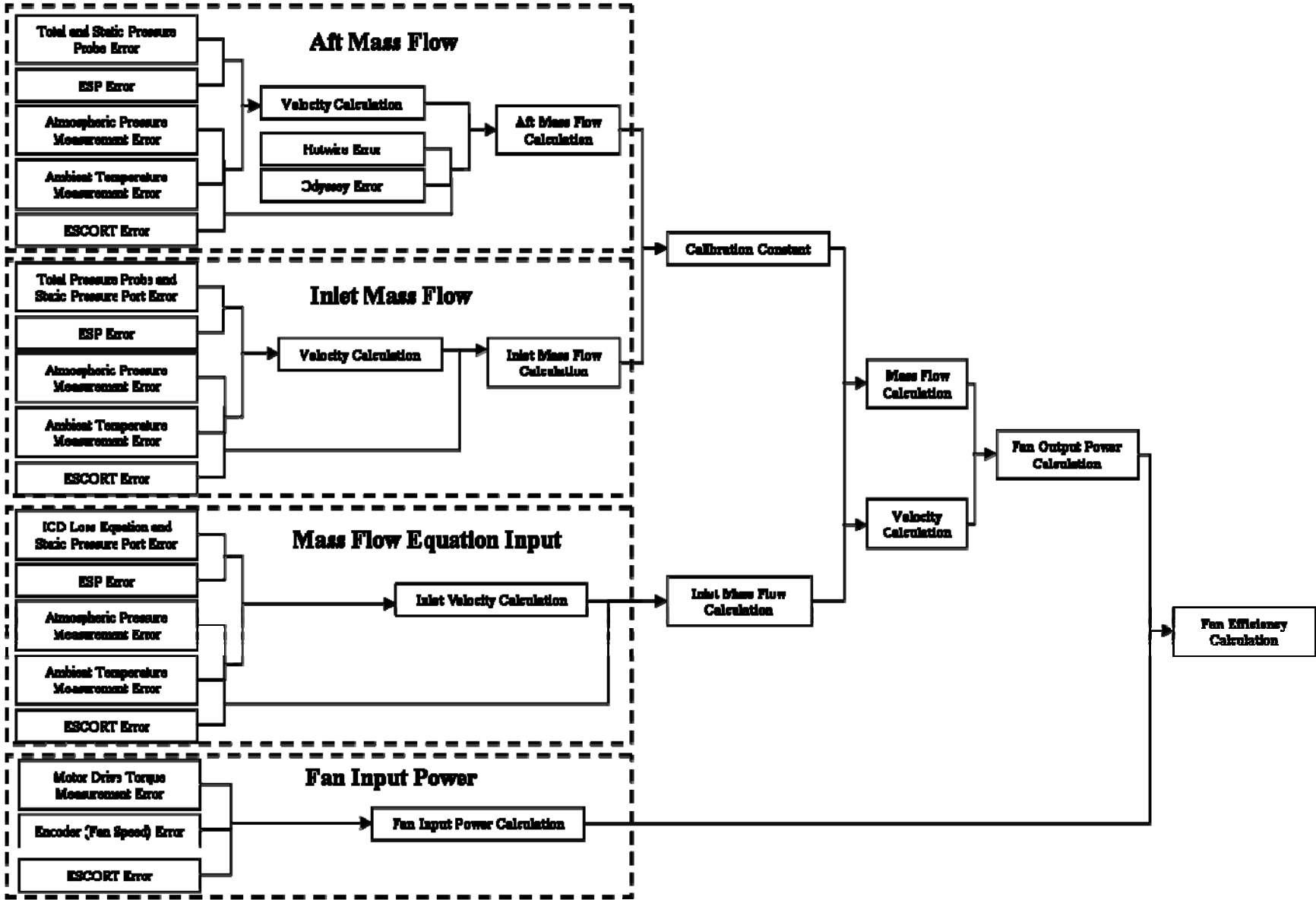


Figure 6.—Error Contributions

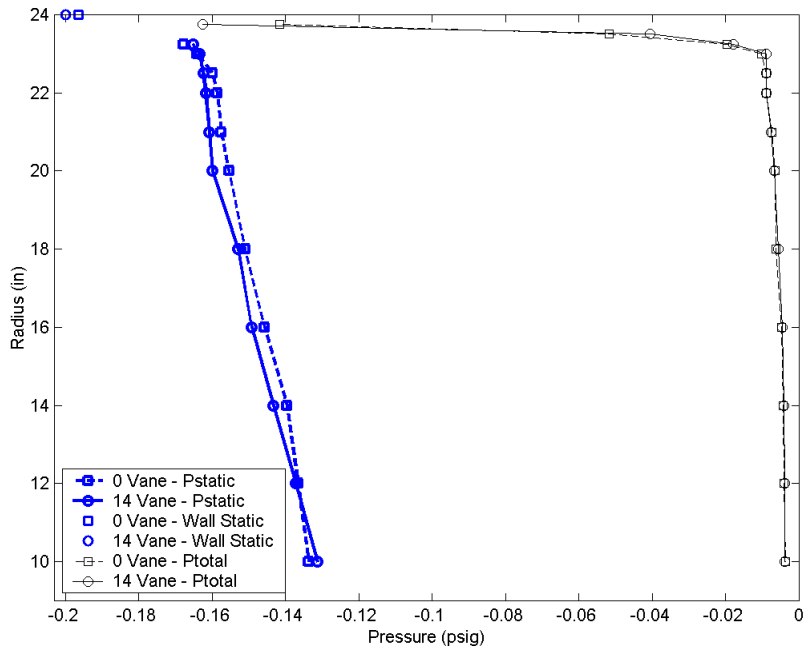


Figure 7.—Inlet Total and Static Pressure Traverses at 1800 RPM_C

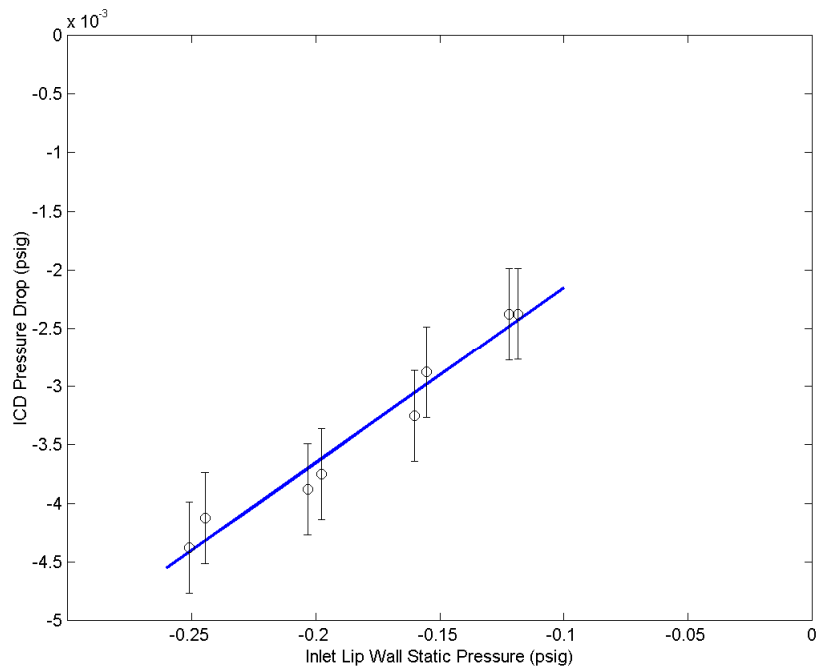


Figure 8.—ICD Pressure Drop data and linear fit
 $\Delta P_{\text{loss}} = 0.015P_s^g + 0.0007$

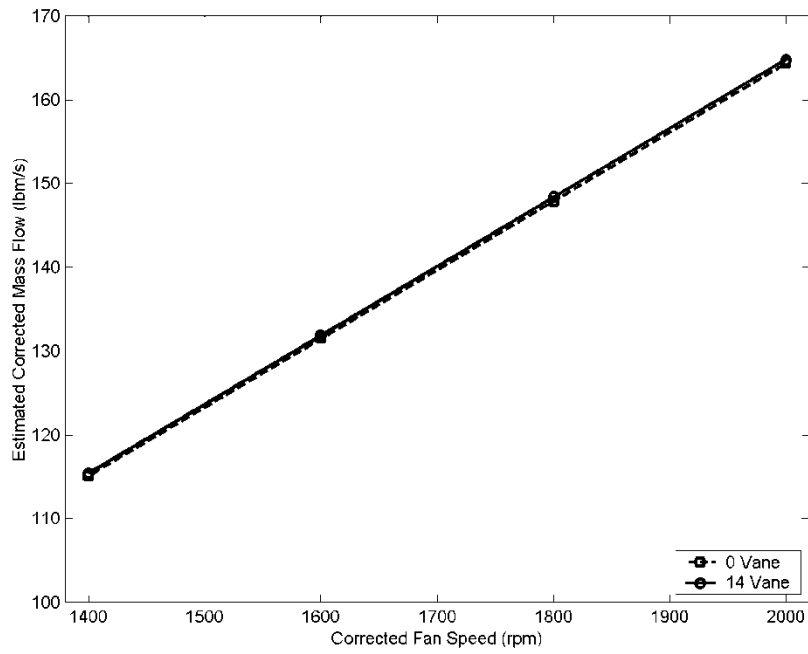


Figure 9.—Estimated Inlet Mass Flow with and without stator vanes
Uncertainty is $\pm 0.34 \text{ lb}_m/\text{s}$

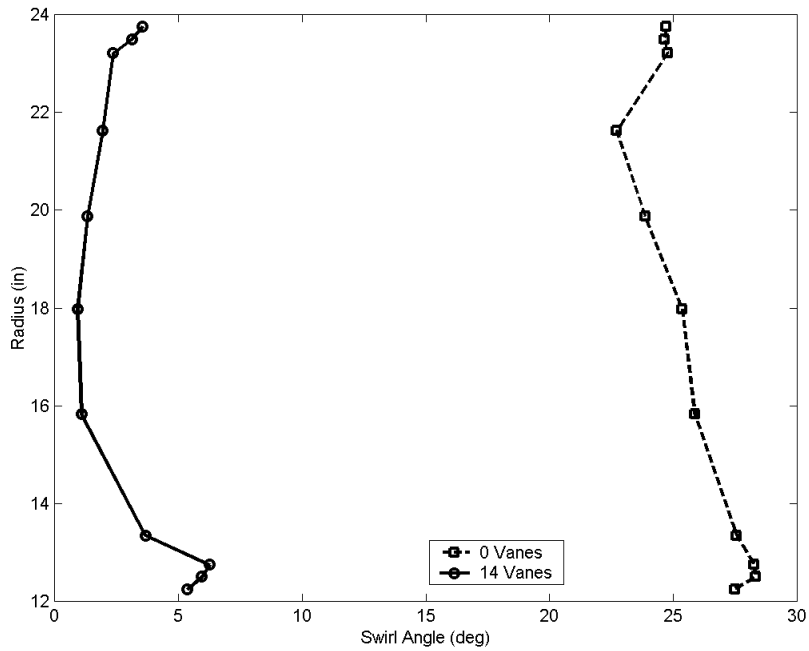


Figure 10.—Aft Section Swirl Angle at 1800 RPM_c

Aft Flow

Aft Swirl Angle

The swirl angle was measured in the aft section with a hot-film probe to examine the effect of the stator vanes on the swirling flow, as well as to determine the axial velocity component used in the axial mass flow calculations. The measured swirl angle in the aft section is shown below in Figure 10. The addition of 14 stator vanes spaced 1 chord behind the rotor reduced the swirl angle by about 20°, but not all the way to zero.

Aft Flow Mapping

Aft flow mapping was done in detail with the total pressure rake. The rake was rotated around the duct in increments of 45° to give 8 circumferential measurement locations, as shown in Figure 2. These 8 circumferential locations combined with the 6 radial pressure measurement locations on the rake give 48 free-stream total pressure measurements.

Additional total pressure measurements were taken with PACS at fixed locations to define the hub and outer wall boundary layers. Two measurements were taken to define the hub boundary layer, while three measurements were taken to define the outer wall boundary layer. These measurements were taken at the 270° circumferential location to measure behind an upstream stator vane and at 180° to measure between two upstream stator vanes. The 58 boundary layer and free-stream total pressure measurements were used to map the flow exiting the ANCF duct.

Static pressure measurements were also taken with PACS traverses at the 180° and 270° circumferential locations. These measurements were used to define the aft static pressure profiles. The measurement locations were identical to those of the free-stream and boundary layer total pressure measurements.

The total and static pressure measurements were used in conjunction with Equation (2) to obtain a Mach number at each location. The Mach number and flow angle were then used to calculate a corrected axial velocity at each of the total pressure measurement locations. This corrected axial velocity was mapped and is shown below in the contour plots of Figure 11.

Since the 8 circumferential rake locations overlap the 14 stator vanes twice, the plots with the stator vanes installed show a flow variation that repeats itself around the duct. This flow variation is an example of spatial aliasing. The data can then be assumed to be periodic about each stator vane, and the plots can be collapsed to show the flow variation over two stator periods, as shown below in Figure 12. While the flow without stator vanes is fairly uniform, the figures on the right, the addition of stators causes variations in the flow that are periodic about the stators, as shown in the figures on the left. The stator vanes create a flow separation, and slower flow, near the center-body.

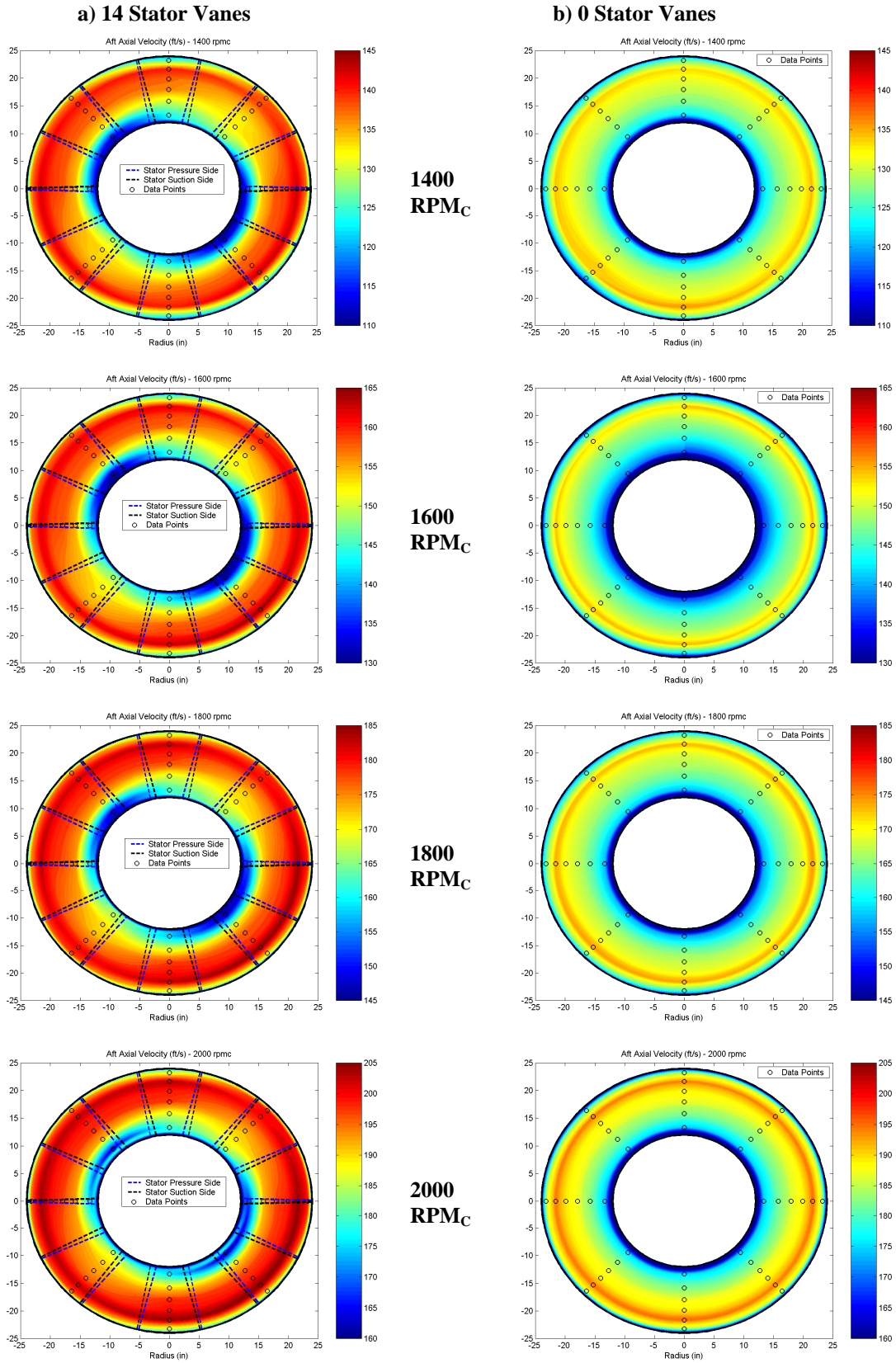


Figure 11.—Aft Axial Corrected Velocities, ft/s, with (a) and without (b) Stator Vanes

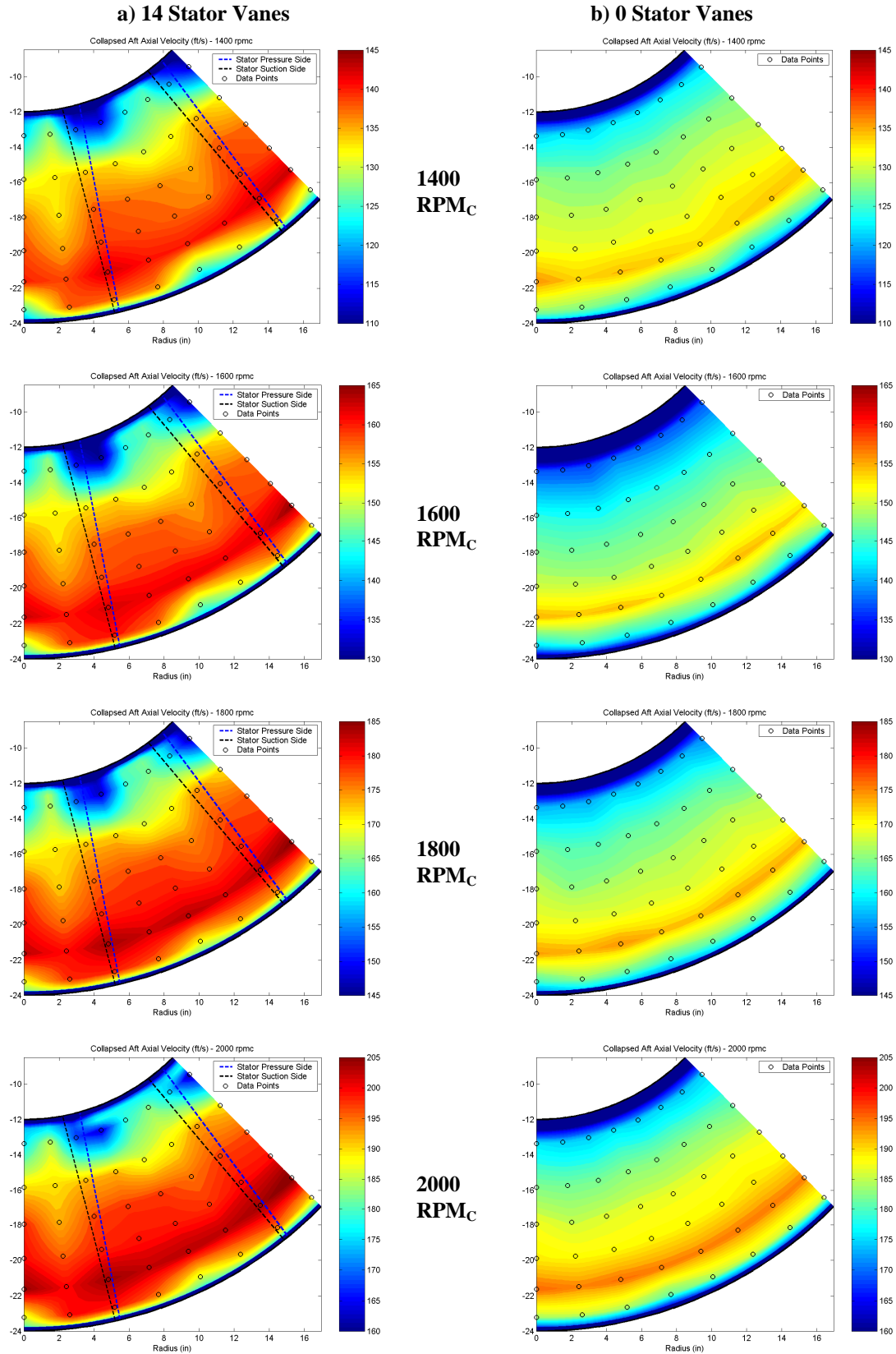


Figure 12.—Collapsed Aft Axial Corrected Velocities, ft/s, with (a) and without (b) Stator Vanes

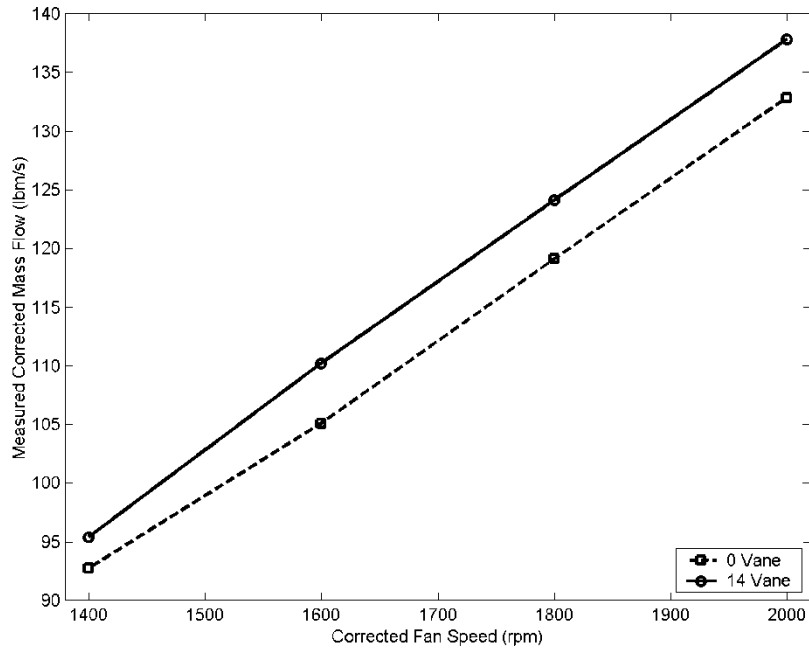


Figure 13.—Aft Measured Mass Flow
 Uncertainty is $\pm 2.1 \text{ lb}_m/\text{s}$

Aft Duct Mass Flow Calculation

The mass flow at the exit plane of the exhaust duct was calculated using Equations (3) and (4). The 6 radial locations and 8 circumferential locations give 48 different points. The Mach number of the flow at that location was calculated from the total and static pressure corresponding to each of these points. The aft duct area was divided into 8 pie sections, and then subdivided into 6 rings to give each measurement an area. The mass flow through the boundary layers was similarly divided into two additional rings around the hub and 3 additional rings at the outer wall. These rings were subdivided with the two circumferential traverses to map the boundary layer around the duct. These areas were used in conjunction with the Mach number, ambient temperature and atmospheric pressure to calculate the mass flow exiting the duct. The mass flow for each configuration at each of the four corrected fan speeds is shown below in Figure 13.

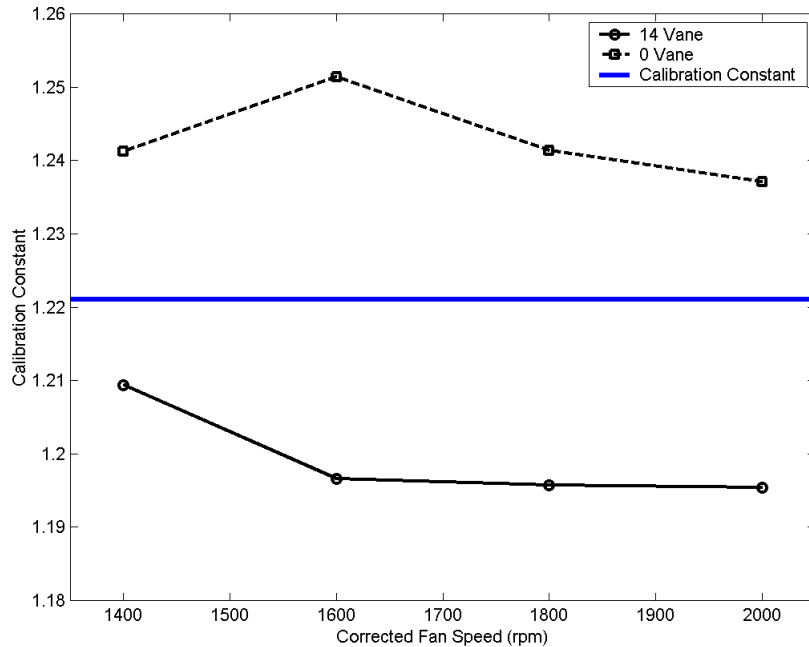


Figure 14.—Calibration Constant
Uncertainty is ± 0.023

Mass Flow and Fan Performance

Calibration Constant

The calibration constant, defined in Equation (1), is the result of dividing the estimated inlet mass flow by the measured aft mass flow. The calibration constant for each configuration and fan speed is shown below in Figure 14. The average of these calibration constants was found to be 1.221. Since the calibration constants have an uncertainty of ± 0.023 , a higher order correlation will not improve the accuracy. Although the correlation is sufficient for a single configuration, the difference in flow with and without stator vanes creates an offset between the calibration constants that is twice as large as the uncertainty, and is yet unexplained.

Fan Performance and Efficiency

The ANCF's input power is calculated from fan speed and torque measurements, while the output power is calculated from the flow measurements. The calculation of the fan's input power does not take into account bearing losses. The fan performance is shown below in Figure 15. While the input power is slightly higher without stator vanes, the output power is lower. Therefore, the fan efficiency is approximately 10% lower when the stator vanes are removed. This inefficiency is due to the energy lost swirling flow and the thicker boundary layers. The fan efficiency over the range of fan speeds for each configuration is shown in Figure 16.

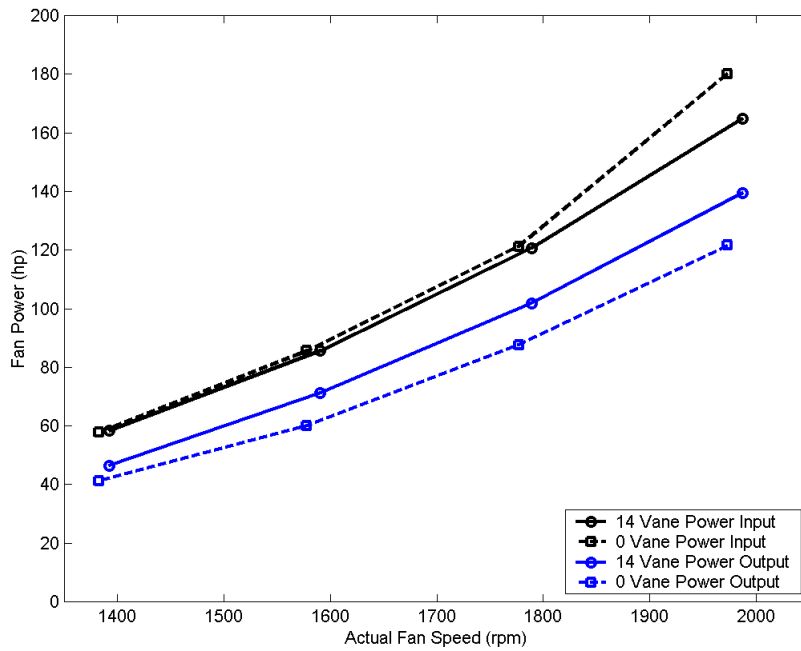


Figure 15.—Fan Performance

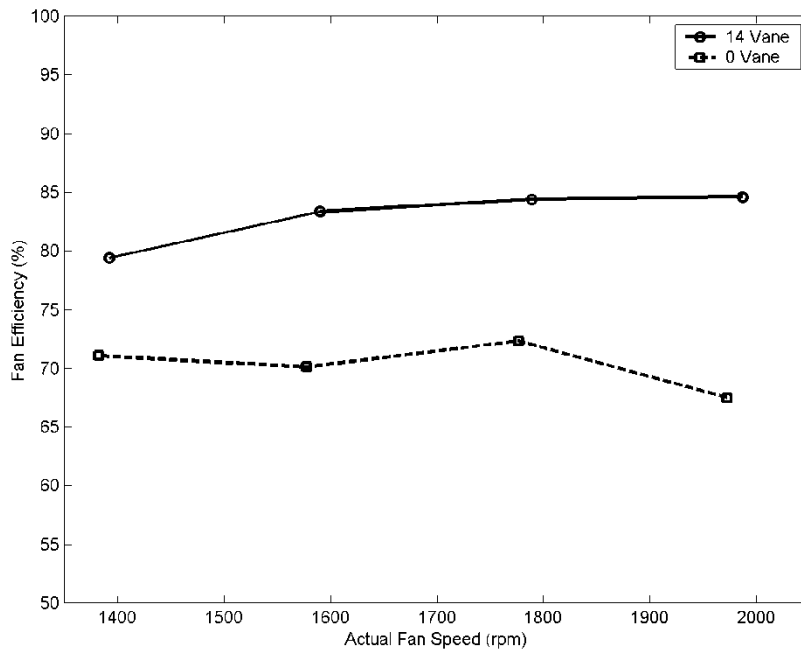


Figure 16.—Fan Efficiency

Summary

The mass flow correlation used was demonstrated to be an accurate method for correlating inlet lip wall static pressure measurements to mass flow. The fan performance can be analyzed in future ANCF configurations without taking the time for detailed flow measurements and calculations. The inlet lip wall static pressure measurements allow for acoustics and flow to be analyzed simultaneously.

References

1. Heidelberg, L.J., Hall, D.G., Bridges, J.E., and Nallasamy, N., “A Unique Ducted Fan Test Bed for Active Noise Control and Aeroacoustics Research”, NASA TM-107213, also AIAA-96-1740.
2. Loew, R.A., Lauer, J.T., McAllister, J., and Sutliff, D.L., “The Advanced Noise Control Fan”, NASA/TM-2006-214368, also AIAA-2006-3150, Nov 2006.
3. McAllister, J., Loew, R.A., Lauer, J.T., and Sutliff, D.L., “The Advanced Noise Control Fan Baseline Measurements”, AIAA 2009-624-779.
4. The American Society of Mechanical Engineers Performance Test Code: Pressure Measurement. ASME PTC 19.2-1987.
5. W. Gracey, W. Letko, and W. R. Russell, “Wind Tunnel Investigation of a Number of Total-Pressure Tubes at High Angles of Attack,” NACA TN 2331, Apr. 1951.
6. Holman, J. P., Experimental Methods for Engineers: Seventh Edition, McGraw-Hill, pp. 331-340, 2001.
7. The American Society of Mechanical Engineers Performance Test Code: Test Uncertainty. ASME PTC 19.1-2005.

REPORT DOCUMENTATION PAGE			Form Approved OMB No. 0704-0188		
<p>The public reporting burden for this collection of information is estimated to average 1 hour per response, including the time for reviewing instructions, searching existing data sources, gathering and maintaining the data needed, and completing and reviewing the collection of information. Send comments regarding this burden estimate or any other aspect of this collection of information, including suggestions for reducing this burden, to Department of Defense, Washington Headquarters Services, Directorate for Information Operations and Reports (0704-0188), 1215 Jefferson Davis Highway, Suite 1204, Arlington, VA 22202-4302. Respondents should be aware that notwithstanding any other provision of law, no person shall be subject to any penalty for failing to comply with a collection of information if it does not display a currently valid OMB control number.</p> <p>PLEASE DO NOT RETURN YOUR FORM TO THE ABOVE ADDRESS.</p>					
1. REPORT DATE (DD-MM-YYYY) 01-11-2009		2. REPORT TYPE Technical Memorandum		3. DATES COVERED (From - To)	
4. TITLE AND SUBTITLE Advanced Noise Control Fan Aerodynamic Performance			5a. CONTRACT NUMBER		
			5b. GRANT NUMBER		
			5c. PROGRAM ELEMENT NUMBER		
6. AUTHOR(S) Bozak, Richard, F., Jr.			5d. PROJECT NUMBER		
			5e. TASK NUMBER		
			5f. WORK UNIT NUMBER WBS 561581.02.08.03.18.02		
7. PERFORMING ORGANIZATION NAME(S) AND ADDRESS(ES) National Aeronautics and Space Administration John H. Glenn Research Center at Lewis Field Cleveland, Ohio 44135-3191			8. PERFORMING ORGANIZATION REPORT NUMBER E-17070		
9. SPONSORING/MONITORING AGENCY NAME(S) AND ADDRESS(ES) National Aeronautics and Space Administration Washington, DC 20546-0001			10. SPONSORING/MONITOR'S ACRONYM(S) NASA		
			11. SPONSORING/MONITORING REPORT NUMBER NASA/TM-2009-215807		
12. DISTRIBUTION/AVAILABILITY STATEMENT Unclassified-Unlimited Subject Category: 01 Available electronically at http://gltrs.grc.nasa.gov This publication is available from the NASA Center for AeroSpace Information, 443-757-5802					
13. SUPPLEMENTARY NOTES					
14. ABSTRACT The Advanced Noise Control Fan at the NASA Glenn Research Center is used to experimentally analyze fan generated acoustics. In order to determine how a proposed noise reduction concept affects fan performance, flow measurements can be used to compute mass flow. Since tedious flow mapping is required to obtain an accurate mass flow, an equation was developed to correlate the mass flow to inlet lip wall static pressure measurements. Once this correlation is obtained, the mass flow for future configurations can be obtained from the non-intrusive wall static pressures. Once the mass flow is known, the thrust and fan performance can be evaluated. This correlation enables fan acoustics and performance to be obtained simultaneously without disturbing the flow.					
15. SUBJECT TERMS Noise; Fan; Aerodynamic					
16. SECURITY CLASSIFICATION OF:			17. LIMITATION OF ABSTRACT	18. NUMBER OF PAGES 25	19a. NAME OF RESPONSIBLE PERSON STI Help Desk (email:help@sti.nasa.gov)
a. REPORT U	b. ABSTRACT U	c. THIS PAGE U			UU

